ELSEVIER

Journal of Molecular Catalysis A: Chemical 173 (2001) 61–74

JOURNAL OF MOLECULAR CATALYSIS A: CHEMICAL

www.elsevier.com/locate/molcata

High resolution TEM studies on palladium nanoparticles

M. José-Yacamán [a,b,*], M. Marín-Almazo [c], J.A. Ascencio [c]

[a] *Department of Chemical Engineering, Texas Materials Institute Center for Nano and Molecular Technology, University of Texas at Austin, Austin, TX 78712-1062, USA*

[b] *Instituto de Física, Universidad Nacional Autónoma de México, Apdo. Postal 20-364, Del. Álvaro Obregón 01000, D.F., Mexico*

[c] *Instituto Nacional de Investigaciones Nucleares, Ámsterdam 46-202, Hipódromo Condesa, 06100 México, D.F., Mexico*

Received 16 October 2000; received in revised form 26 February 2001; accepted 28 February 2001

Abstract

In the present work, we discuss the analysis of Pd nanoparticles in the range of 1–5 nm using high resolution electron microscopy (HREM). Particles were grown using colloidal methods. The principles of the observation of HREM images and their study using the corresponding FFT of the images are discussed.

The results show that particles have the following shapes: FCC cubo-octahedrons, icosahedrons, truncated decahedrons and single-twinned FCC configuration. Each one of those structures is discussed and images are shown. We also found that a fraction of the particles corresponds to a short range ordered amorphous phase. The future of HREM observations of nanoparticles is also discussed.

Keywords: Palladium nanoparticles; Electron microscopy of nanoparticles; Nanomorphology; Crystalline structure of palladium nanoparticles

1. Introduction

There is a growing interest in many areas of the science in understanding the properties of nanomaterials. A particularly interesting application is the possibility of using arrays of nanoparticles for fabrication of single electron tunneling devices [1].

The field of catalysis however is one in which the nanosciences have been applied for many years. Indeed, the goal of having a catalyst, with the maximum active area exposed to a chemical reaction, has produced enormous amount of research in nanoparticles. Particularly, the metal nanoparticles study is a very important field in catalysis [2].

Electron microscopy is one of the techniques that have played a major role on studding nanoparticles. Since the early conventional bright field images and the intermediate resolution dark field techniques [3], to the high-resolution atomic images of nanoparticles [4] the results have shown that indeed the nanoparticles (Pt and Au mainly), in the range of a few nanometers, can have well-defined crystal structures. Even if sometimes the structure is not the one corresponding to the bulk metal.

More recently, the High Angle Annular Dark Field images or Z-contrast has demonstrated the existence of clusters ∼1 nm [5]. However, this technique provides only indirect evidence of the atomic arrangements in the particles. High resolution electron microscopy (HREM) still appears as a very powerful technique to study nanoparticles and their internal structure.

Among the most interesting metals to study is the palladium, which acts for instance as excellent catalyst for hydrogenation of unsaturated hydrocarbons [6] and

* Corresponding author. Tel.: +1-512-232-9111.
E-mail address: yacaman@che.utexas.edu (M. José-Yacamán).

1381-1169/01/$ – see front matter
PII: S1381-1169(01)00145-5

has many other applications such as environmental catalysts.

In the present work, we report a study of the structure of Pd clusters grown by colloidal methods using high resolution TEM, fast Fourier transforms of images, modeling of the structure and molecular dynamics calculations. Palladium clusters have been studied by a number of groups using TEM (see for instance, [7–10]). However, HREM images of very small clusters ~1–1.5 nm have not been discussed in the literature.

2. Theoretical basis of high resolution TEM images

In order to understand the basis of images of nanoparticles, we will present in this section some theoretical background. In a TEM, electrons are scattered in the sample by a small angle between 10^{-1} and 10^{-2} rad. Therefore, this is a forward scattering geometry in which we can use the small angle approximation.

The wave equation for the electrons can be written as

$$\nabla^2\psi(r) + k^2\psi(r) = 0, \tag{1}$$

where k is the magnitude of the wave number $(1/\lambda)$ and (r) is the wave function. Besides k is defined in a quantum mechanics form as

$$k^2 = (2me/\hbar)[E_0 + \phi(r)], \tag{2}$$

where m and e are the mass and charge of the electron, respectively, while $\hbar$ is the Planck constant, E_0 corresponds to the electron acceleration voltage and $\phi(r)$ represents the potential (electrostatic) field. As shown by Spence [11], the refractive index of the sample can be approximated as

$$n = \frac{k}{k_0} \approx 1 + \frac{\phi(r)}{2E_0}, \tag{3}$$

if we consider that typically the electrostatic potential is ~5–20 eV and the accelerating voltage is approx. -2×10^5 eV, then the refraction index is very close to the unity. This approximation, of course, is not good for solids with a higher electrostatic potential or for lower voltages.

If we assume that only the wave phase is changed when the electrons cross the specimen, the phase change for the electrons moving in the z direction is proportional to

$$\phi(x, y) = \int \phi(x, y, z)\,\mathrm{d}z,$$

the sample can be then consider to have a transmission function $q(x, y)$, which multiplies the incoming wave by a factor

$$q(x, y) = \mathrm{e}^{-\mathrm{i}\sigma\phi(x,y)}, \tag{4}$$

where σ is the interaction constant

$$\sigma = \frac{2\pi me\lambda}{h^2}. \tag{5}$$

The Eq. (4) is called the phase object approximation (POA), which has very useful in calculating images of thin crystals [12].

We can even make a linear approximation and the transmission function becomes

$$f(x, y) \cong 1 - \mathrm{i}\sigma\phi(x, y). \tag{6}$$

This is known as the weak phase object approximation (WPOA). However, it is clear that those approximations might fail for small particles. For instance, in the case of gold, a few atom clusters can already produce inelastic scattering or changes in the electron direction due to the scattering and even refraction effects. The same situation is valid for palladium. These approximations however are very useful for understanding qualitatively the images of small particles.

The intensity of the diffraction pattern I_D will be given by

$$I_\mathrm{D}(u, v) = \delta(u, v) + \sigma^2\Phi^2(u, v) \times \left(\frac{\sin(a\pi u)}{\pi u}\frac{\sin(b\pi v)}{\pi v}\right)^2, \tag{7}$$

where δ is the delta function in two dimensions, Φ the Fourier transform of $\phi(x, y)$, while u and v are the coordinates in the diffraction plane and a and b define the size of the aperture used to select the diffracted area.

The final intensity that will be observed in the image plane $I_\mathrm{I}(x, y)$, will be given by the Fourier transform of

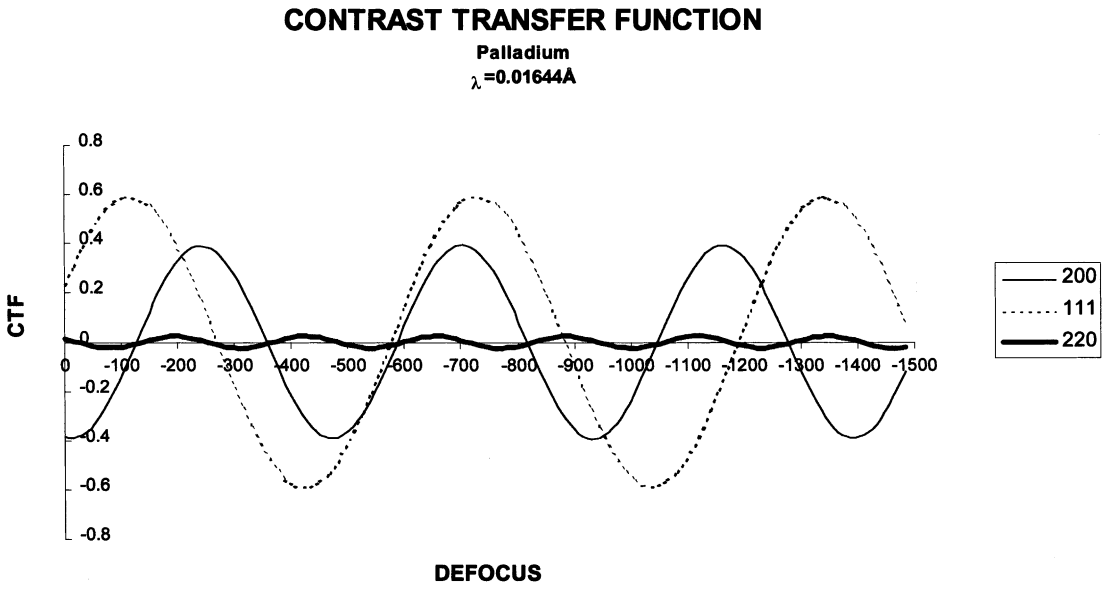

Fig. 1. Contrast transfer function plotted vs. defocus of the objective lens for the three principal reflections of Pd; (1 1 1), (2 0 0) and (2 2 0).

the wave function for the diffraction pattern and will be given by

$$I_{\mathrm{I}} = 1 - 2\sigma\phi(x, y) \times \Im\{\sin\gamma\}, \tag{8}$$

where γ is the phase shift of the electron waves at the focal plane and is given by

$$\gamma = \frac{\pi}{2}(C_{\mathrm{s}}\alpha^4 - 2\Delta f\alpha^2), \tag{9}$$

where α is the aperture angle, f the defocus and C_{s} corresponds to the spherical aberration coefficient.

Eq. (8) contains the periodicity expected for the image. One critical parameter to find out the best imagining conditions for particles is to plot the value of the $\sin\gamma$ function (contrast transfer) versus defocus. The results are shown in Fig. 1. The calculation in Fig. 1 was performed for a JEOL 4000 EX microscope with a limit resolution of ~1.7 Å. In the so-called Scherzer defocus [13] ($\Delta f = -405$ Å), the columns of atoms appear as black dots, and the (1 1 1) planes will tend to have better contrast than the (2 0 0) crystallographic planes. However, for a defocus of $\Delta f =\sim 702$ Å corresponding to a second maximum the columns of atoms will appear as white dots and both (1 1 1) and (2 0 0) planes will have about the same contrast. Therefore, this condition appears more convenient for imaging Pd particles.

On the other hand, it is often convenient to obtain the Fourier transform of a high resolution image using a CCD camera to collect the image and then calculating the Fourier transform, Tomita et al. [14] have shown that the intensity of the transform is given by

$$L(u, v) = \delta(u, v) + 4\sigma^2\Phi^2(u, v)\sin^2\gamma \times \left(\frac{\sin(a\pi u)}{\pi u}\frac{\sin(b\pi v)}{\pi v}\right)^2, \tag{10}$$

where a and b represent the dimensions of the area in which we obtain the FFT. As can be seen by comparing (9) and (6), when sin = ±1, i.e. at Scherzer defocus, the FFT of the image is identical to the diffraction pattern. However, this is only true if the WPOA approximation is valid and the defocus is at one of the maximum values.

Suppose now that the crystal is very thin or the sample is a strong dynamical scatter. In this case, we have to use the dynamical theory of electron diffraction which makes the situation much more complex.

According to the standard dynamical diffraction theory [15,16], the electron wave at the exit of the

sample after traveling a distance z is given by

$$\phi(z) = \sum_g \sum_j A^{(j)} C_g^{(j)} \, e^{2\pi i k_0^{(j)} z} \, e^{2\pi i g r}, \quad (11)$$

where $A^{(j)}$ are combination constants, $C_g^{(j)}$ is the amplitude of the j wave and $k_0^{(j)}$ is the component of the wave vector along the z direction.

Assuming coherent interference the intensity is then given as

$$I(r) = \sum_{g'} \sum_{g''} \Phi_{g'} \Phi_{g''}^* \, e^{2\pi i (g''-g')r} \, e^{i(\gamma_{g''}-\gamma_{g'})}, \quad (12)$$

where

$$\Phi_g = \sum_j A^{(j)} C_g^{(j)} \, e^{2\pi i k_0^{(j)} z}. \quad (13)$$

However, in most realistic cases the specimen is illuminated by a partially coherent wave. Then, we have to introduce the transmission function $T(g', g'')$ that reflects the electron optical characteristics of the microscope.

So the intensity at the exit of the sample is given by

$$I(r) = \sum_{g'} \sum_{g''} T(g'', g') \Phi_{g''} \Phi_{g'}^* \, e^{2\pi i (g''-g')r}, \quad (14)$$

and the transmission function is given by

$$T(g'', g') = e^{-i(\gamma_{g'}-\gamma_{g''})} E_d E_f P E_k,$$

where E_d is related to the beam divergence, E_f is related to the chromatic aberration and P is the aperture function that can be used as $P = 1$, besides E_d is expressed as

$$E_d = e^{-(\pi\alpha_0/\lambda)^2 [C_s \lambda^3 (g''^3 - g'^3) - \Delta f \lambda (g''-g')^2/u],} \quad (15)$$

E_f is given by

$$E_f = e^{-(\pi \Delta\lambda/2)^2 (g''-g')^2/u}. \quad (16)$$

Supposing that we now take the Fourier transform of the high-resolution image, which is contained in Eq. (13). This will be

$$F(\vec{g}) = \sum_{g'} \sum_{g''} T(g'', g') \Phi_{g''} \Phi_{g'}^*, \quad (17)$$

with

$$g = g'' - g'$$

and the intensity is

$$I_T = F(g) F^*(g)$$

The nature of the summation indicates that distance between spots in a FFT is still equal to g. Therefore, even in the dynamical case useful information about the crystallography of a small particle can be obtained by using the FFT of the HREM image. Even though in this case the intensities of the FFT spots are not necessary related to the intensity of diffraction spots. On the other hand, since we can control the size of area in which the FFT is obtained it is possible to obtain crystallographic information on small regions of a nanoparticle.

3. Experimental methods

3.1. Particle preparation

Samples were prepared using modifications for Pd of the methods of Bönnemann et al. [18] and Brust et al. [17]. We started with a portion of 0.1 g of $PdCl_2$, which is mixed with 75 ml of tetrahydrofuran (THF); magnetic agitation is used to produce and homogeneous solution. Then, we added 0.55 ml of 1-dodecanethiol $[CH_3(CH_2)_{11}SH]$ and the same amount of $[LiB(C_2H_5)_3H]$. The reaction is run for 16 h and finally the THF is evaporated. The final product is precipitated on cold ethanol several times to remove the excess of 1-docecanothiol. The resulting structures are particles of Pd metal in which the surface is passivated with an alkyl–thiol molecule.

3.2. Electron microscopy and image processing

Electron microscopy was performed using a JEOL-4000 EX high-resolution microscope with a resolution ~1.7 Å and with a JEOL-2010 EX microscope fitted with an analytical pole piece and a resolution of ~2.0 Å. Samples were prepared on carbon grids for TEM observations. Images were digitized using a high-resolution CCD camera and computer processed to obtain the FFT. The patterns were analyzed to determine the distances. Images of the particles were calculated using the simulaTEM program developed by Beltran del Rio and A. Gomez.

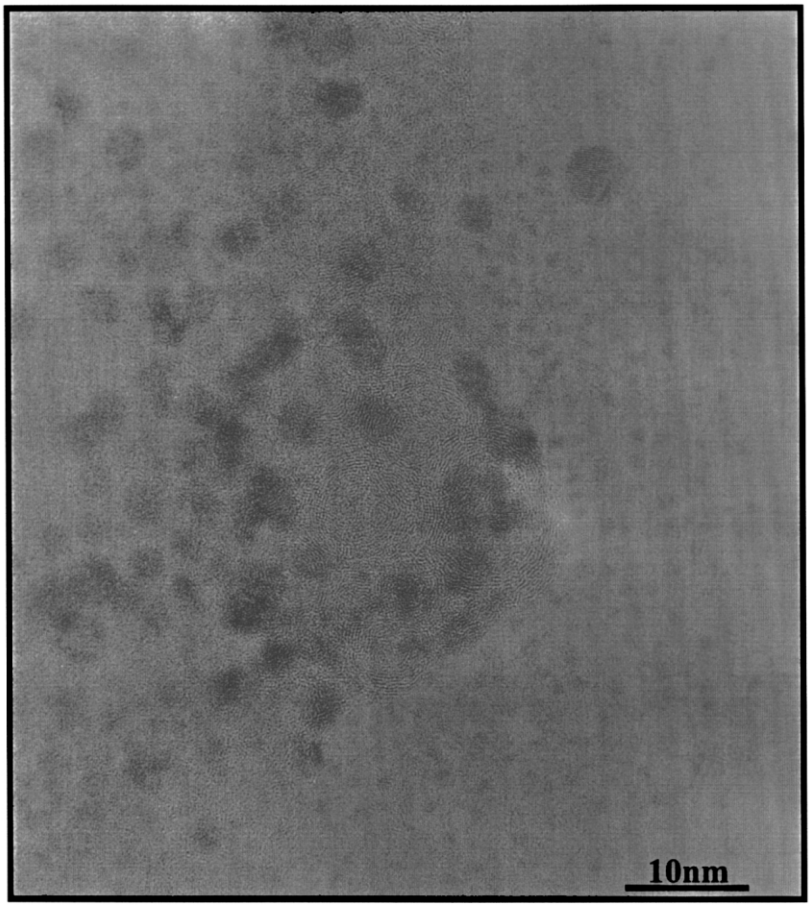

Fig. 2. General view of the Pd nanoparticles that are obtained by the methods explained in the text. Note the bimodal size-distribution.

4. Experimental results

A general view of the Pd particles obtained by our experimental methods is shown in Fig. 2. As can be seen from the image there is a broad size distribution of particles ranging from <1 nm to $\sim$5 nm. However, there is a high preference for the very small clusters. We have made a detailed analysis of all the types of particles that can be observed in the samples. We classified them in several groups: FCC, icosahedral, decahedral and twinned particles. In the following sections, we will discuss each one in the more detail. It should be remembered that our preparation method renders particles whose surface is passivated by an alkyl–thiol molecule. Nevertheless, the passivating agent does not alter the basic shape and geometry of the particle. However, it can produce distortions along some crystal planes.

4.1. FCC cubo-octahedral particles

The first type corresponds to particles with a FCC structure. Fig. 3 shows a few examples: Fig. 3(a) corresponds to a particle of $\sim$1 nm in diameter, which is obtained in the second maximum of contrast corresponding to a condition where the columns of atoms appear as white dots. The particle has a $\langle 1\,1\,0\rangle$ orientation with respect to the electron beam. A slightly larger $\langle 1\,1\,0\rangle$ oriented particle is shown in Fig. 3(b). In Fig. 3(c), a particle with $\langle 1\,0\,0\rangle$ orientation is shown, this particle is around 2 nm in size and it shows clearly the square distribution contrast. Finally, the Fig. 3(d)

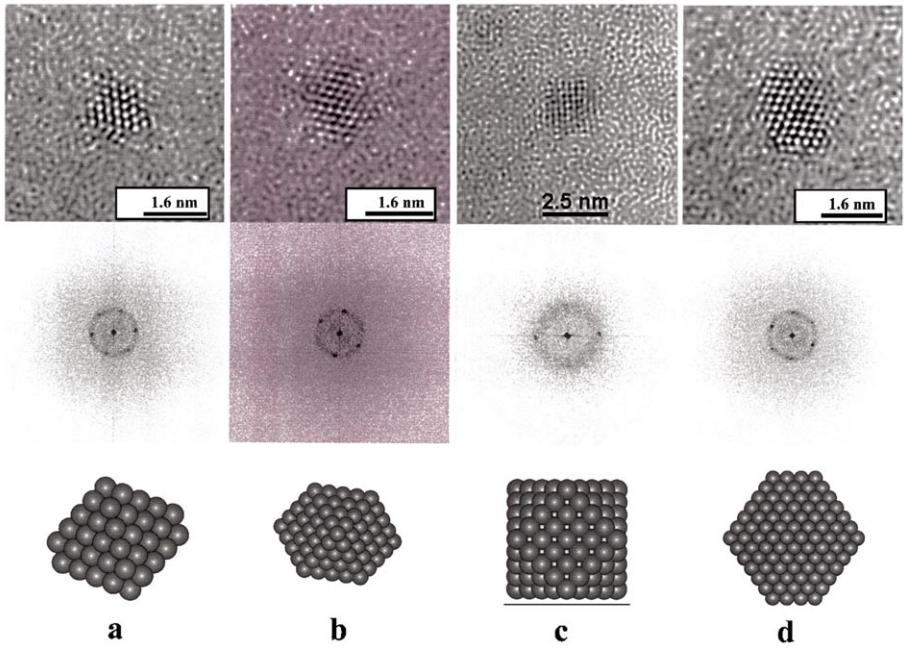

Fig. 3. HREM images of Pd particles with FCC structure (a) and (b) are in a ⟨1 1 0⟩ orientation and (c) is in a ⟨1 0 0⟩ orientation, while (d) corresponds to a particle with a hexagonal profile, which corresponds to a distorted ⟨1 1 0⟩ orientation. The corresponding FFT is included in each case.

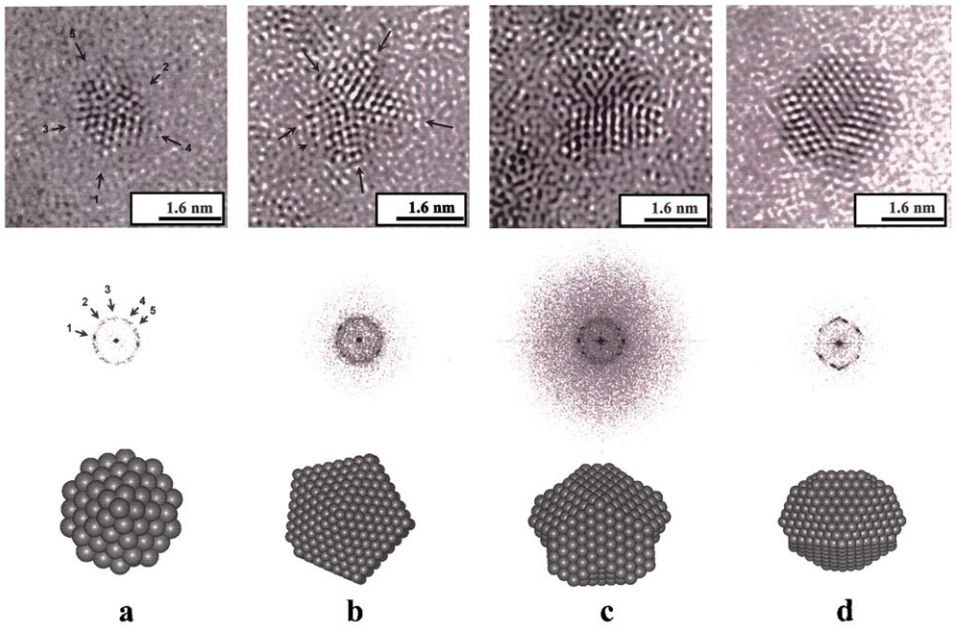

Fig. 6. Sequence of HREM images for decahedral Pd particles showing different orientations with respects to the one five fold axis parallel to the electron beam. A model shows in each case the orientation the corresponding FFT is included in the figure.

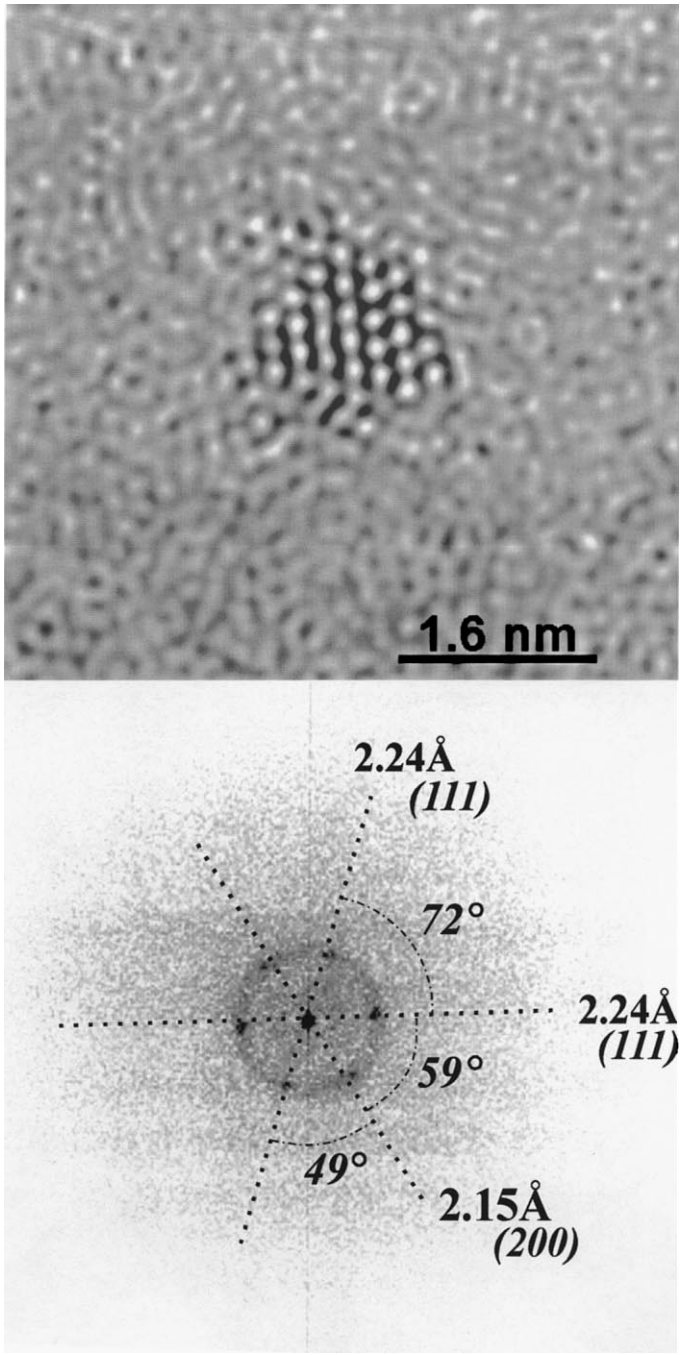

Fig. 4. HREM image of a Pd particle in the ∼1 nm size in which the lattice parameters have been measured. Note that the obtained values of the (2 0 0) planes of 2.15 Å which represent a distortion of 12.5% with respect to the bulk value. Note that the angles are also distorted.

shows an FCC with a well-defined hexagonal shape. It must be remembered that the (2 2 0) reflections for Pd are 1.37 Å, which is below the microscope detection limit and the particles in the ⟨1 1 1⟩ orientation cannot be observed. Therefore, it is clear that Fig. 3(d) does not correspond to a ⟨1 1 1⟩ orientation. The Fig. 3 shows clearly that one of the shapes that particles can assume corresponds to the regular FCC cubo-octahedron or their truncations (such as the tetrakaidecahedron).

We have performed a very careful and detailed measurement of the lattices spacing of the very small particles. The magnification of the microscope was calibrated and then the FFT. The result is shown in Fig. 4 for a particle ∼1 nm.

It is clear that the ⟨2 0 0⟩ planes are distorted and appear with a value of 2.15 Å, this is in contrast with the bulk value of 1.92 Å. Therefore, there is a distortion in the particle of ∼12.5% (expansion) along the ⟨1 0 0⟩ direction. As can be seen from the figure the angles between planes are also distorted and do not correspond to the bulk valves. This is a remarkable fact that contrast very much with gold particles, in which a lattice contraction has been reported [19]. Previous reports by Heinemann et al. [10] for Pd in MgO indicated a lattice expansion to accommodate the misfit. However, in our case the particles are supported on a weak interacting substrate (amorphous carbon).

4.2. Icosahedral particles

Fig. 5 shows images of icosahedral particles: (a)–(c) correspond to particles in five fold orientation

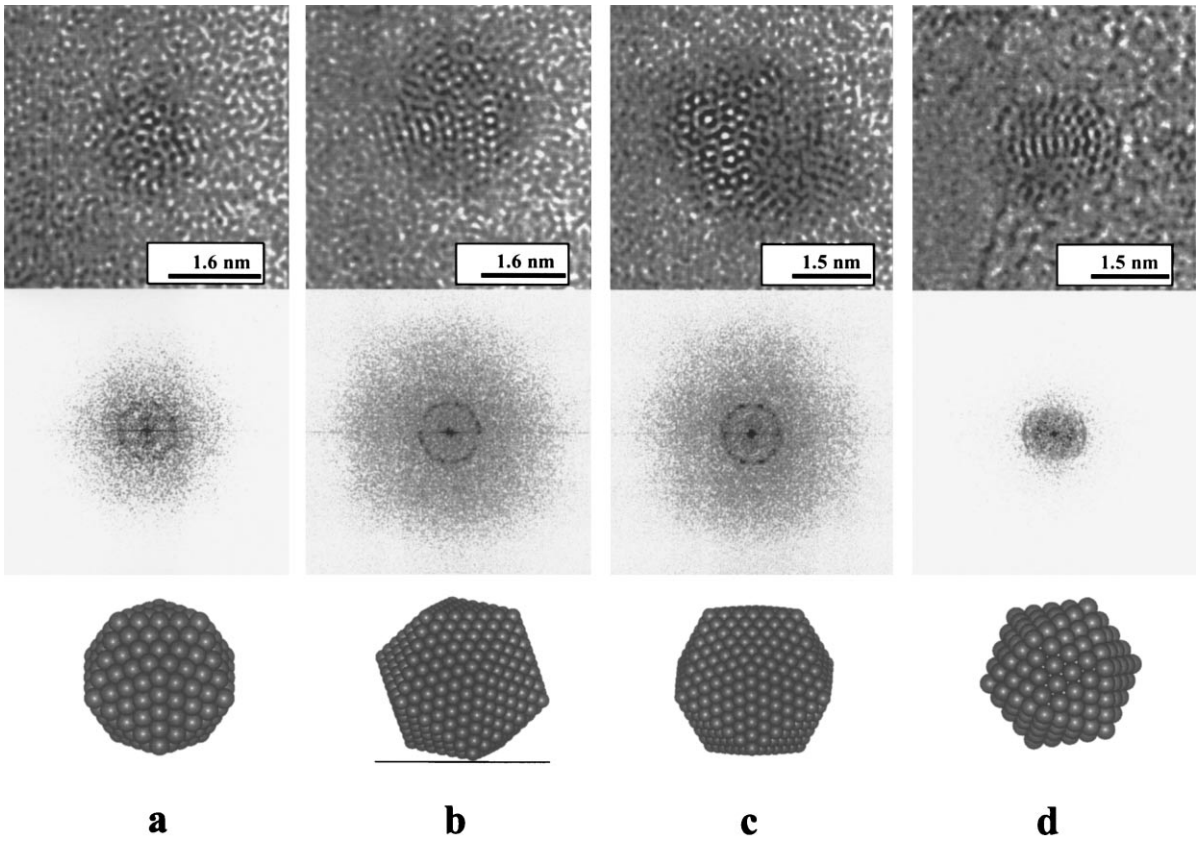

Fig. 5. Sequence of HREM image of icosahedral particles of Pd: (a), (b) and (c) are in a near five fold orientation and (d) is in a two fold orientation. The corresponding FFT is included in each case.

whereas, (d) corresponds to a particle in two fold orientation. The particle in Fig. 5(a) has a size of ∼1 nm and although there are some background noise, in the FFT the 10 spots corresponding to the five fold orientation can be clearly seen. The particles in (b) and (c) are slightly tilted away from the five fold orientation. The particle in (d) corresponds also to a perfect two fold orientation [20,21]. It is interesting to note that in contrast with the case of gold particles in which the five fold orientation is rarely seen, in the case of Pd appears to be the most frequently observed.

4.3. Decahedral particles

The next type of structure corresponds to the truncated decahedra first introduced by Howie and Marks [22]. These particles are shown in Fig. 6 in different orientations. The Fig. 6(a) corresponds to a particle with just ∼1 nm size but it is possible to observe the five tetrahedral twins forming the particle. In each case, the orientation of the particle with respect to the electron beam is shown in the Fig. 6 with the corresponding model.

This kind of particles might have some variants such as the star like pentagon or the rounded pentagon [23]. These particles, besides the (1 1 1) and (1 0 0) facets, have reentrant (1 1 1) facets which further minimize the total energy of the particle. In the case of gold, this configuration shape has been found to be remarkably stable [24]. We also note from the images, in Fig. 6(b), that some of the twin boundaries are incoherent, this is consistent with the previous reports for gold particles by Gao et al. [25]. This produces split on the spots shown in Fig. 6(b). It is however important to mention that in many cases perfect coherent twins are observed such as the case of Fig. 6(a).

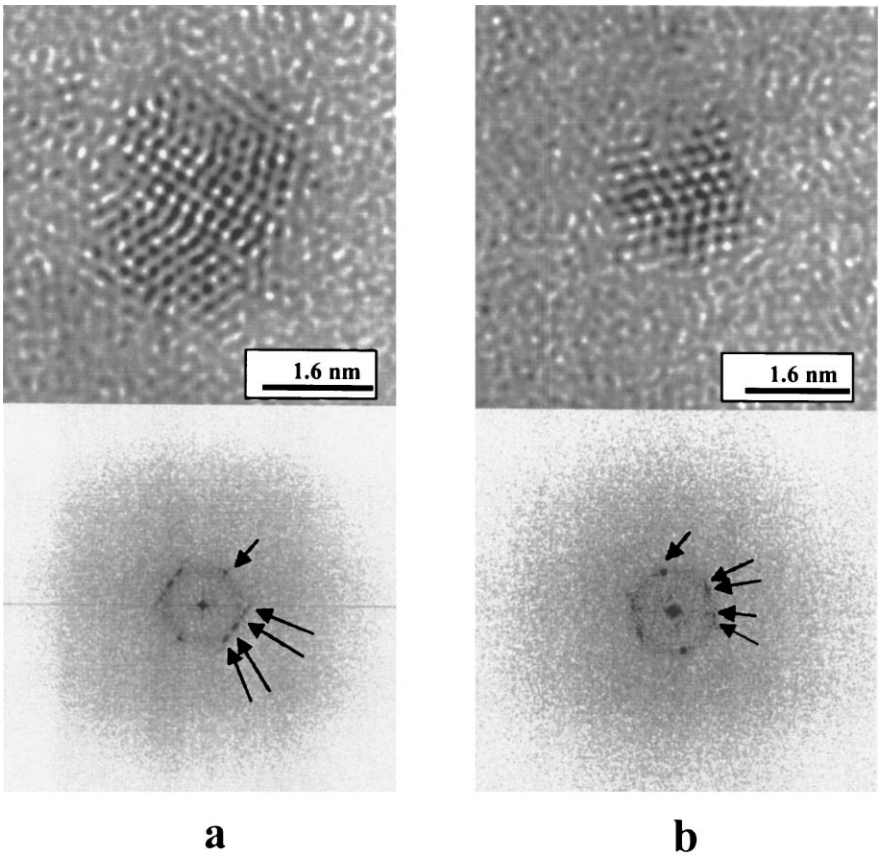

Fig. 7. HREM images of single-twinned Pd particles; note the splitting of the FFT spots indicated in both cases.

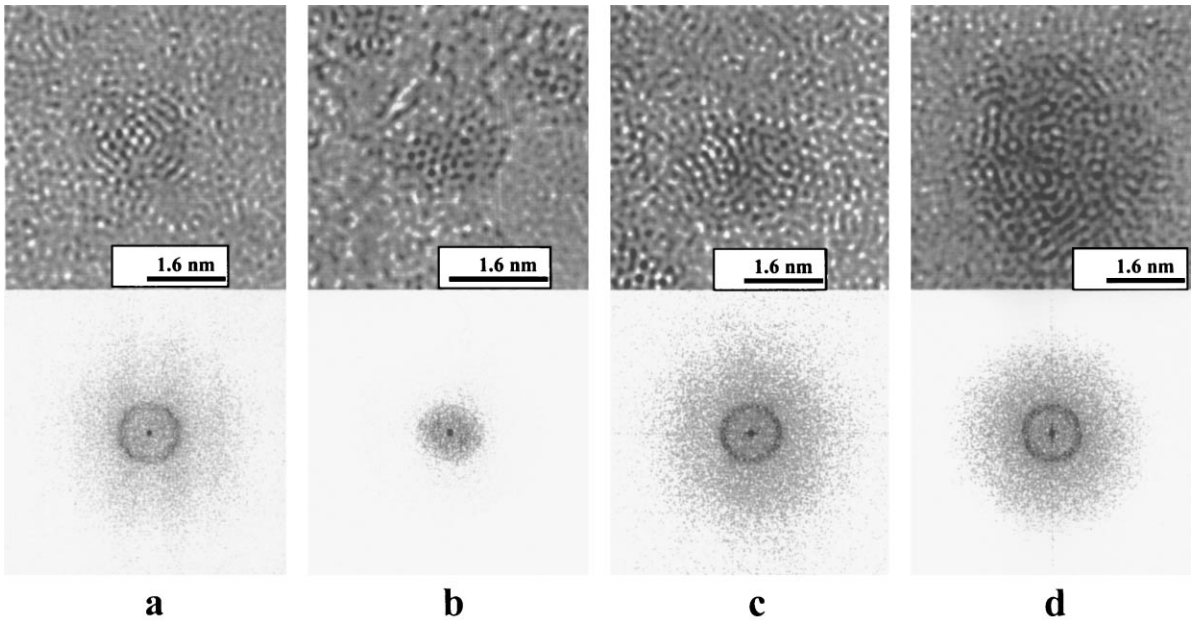

Fig. 8. HREM images of amorphous particles: (a) shows a cluster of ∼1 nm; (b) shows a particle with a well-defined dark contrast in the atomic column; (c) and (d) show larger particles. The FFT is shown in each case.

4.4. Twinned particles

In this section, we will discuss particles that will only have one or two twin boundaries and therefore do not have the pentagonal or icosahedral structure. They are FCC particles, which have developed a twin boundary. Examples of those particles are shown in Fig. 7(a)–(b). In this case again we identified the twins by the FFT. In this case, we see splitting of the spots ⟨1 1 1⟩ spots as shown by the arrows in FFT of Fig. 7(a) and (b). The twin geometry can be more clearly seen in a larger particle as the one corresponding to Fig. 7(a). The smallest twinned particle that was observed was again close to 1 nm in Fig. 7(b). Single-twinned particles remain remarkably stable a do not change to other configurations.

4.5. Amorphous particles

In many cases, we were able to obtain particles in which the geometry could not be established in any sense. In all cases those particles produce noisy and undefined FFT. Examples of those particles are seen in Fig. 8. The particles vary in size but they can be as small as the particle shown in Fig. 8(a), which has a size of ∼1 nm. The Fig. 8(b) shows a particle in which the lines of atoms show strong dark contrast but the FFT shows no indication of ordering. Fig. 8(c) and (d) correspond to larger particles. The subject of amorphous nanoparticles has been subject of a big controversy. However, in a recent calculation by Garzon et al. [26] amorphous structures were found theoretically for the case of gold clusters. In new of those calculations is very likely that the reported particles correspond to short-range order amorphous structures. The Fig. 9 shows some possible models for the amorphous clusters obtained by molecular dynamics simulation. This is the first time, to our knowledge, that small amorphous nanoparticles are found experimentally in the case of Pd.

5. Discussion of nanoparticle geometry

We have shown in the previous section that the nanoparticles of Pd might show four basic shapes: FCC cubo-octahedral, icosahedral, decahedral and twinned. These four geometries appear to have a

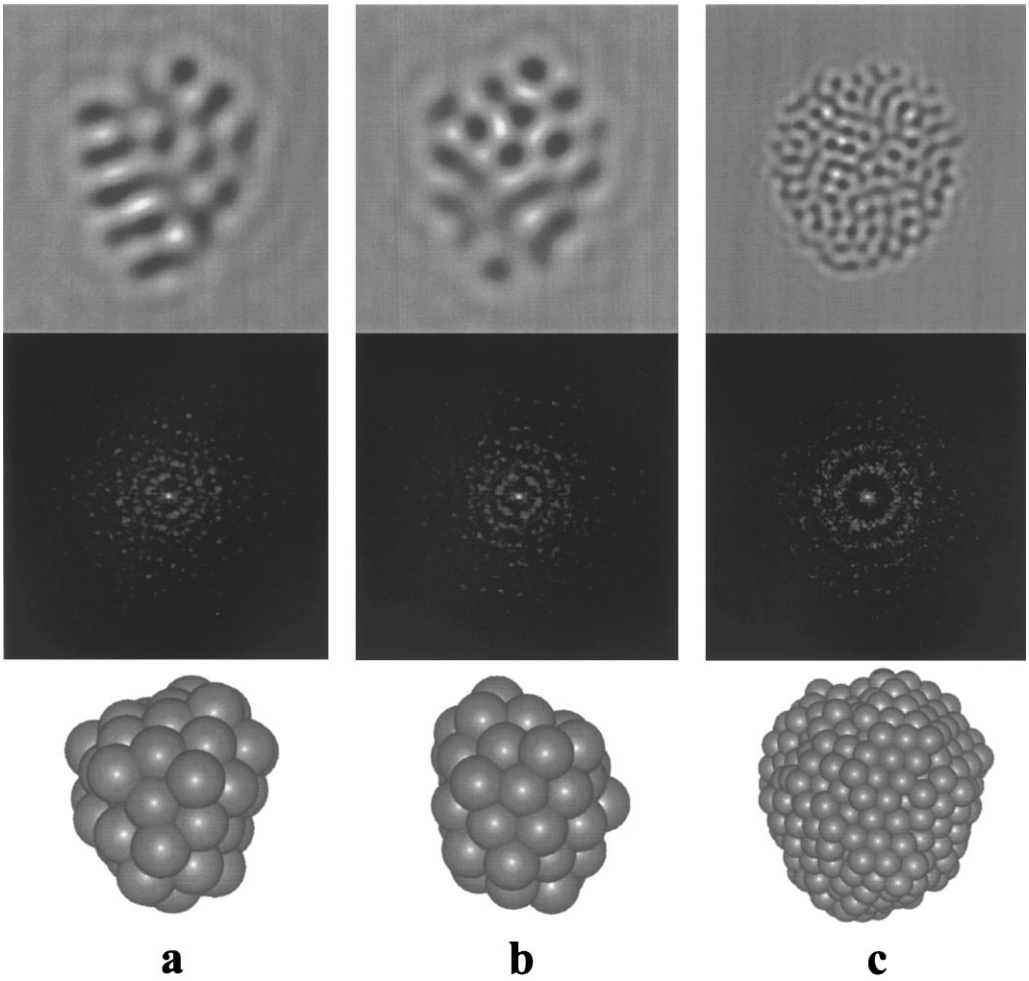

Fig. 9. Theoretical models for the amorphous Pd particles for 55 (a–b) and 561 (c) atoms. The FFT and the simulated image are shown in each case.

similar probability of being observed. There is a very clear reason for that behavior; all those structures correspond to states that have a very similar energy. Therefore, a jump between different states is very likely. In fact, in most growth conditions we will expect that the kinetics will dominate the final shape of the particles. In other words, the equilibrium structures will not be easily achieved. This is an important fact for catalysis. Most methods used to prepare Pd catalyst will not produce equilibrium structures and a distribution of shapes it is expected to be observed.

One of the most remarkable structures is the icosahedron structure. As discussed by Martin [27] the icosahedron is a highly strained structure. The structure is formed by shells and the inter-atomic distance between shells is smaller than those within the shell. Therefore, the icosahedral structure is only expected for very small clusters with a high surface to volume ratio. However, some of the clusters observed in this work can have a relatively large size.

In the case of the decahedral configuration a regular decahedron can be formed by deforming five tetrahedral and a shell structure can be formed. However, the

regular decahedron has a large surface area and internal strain and is not expected to be stable. However, if truncations are introduced it becomes more spherical and therefore more stable. This truncation exposes [1 0 0] faces. An additional truncation of [1 1 1] faces reduces the energy even more. This shape is therefore expected to be more stable than the icosahedral shape. Also the FCC cubo-octahedral particles appear to be truncated and very stable.

It should be emphasized that the facts that particles are surface passivated do not alter the basic shapes observed. One possibility for the future is to look if the passivating molecule could be used to select a given particle shape.

6. Electron microscopy of nanoparticles in the near future

The first pioneering work, of high-resolution analysis on Pd, was made by Renou and Penisson [28] for larger particles since then a lot of progress in the area has been made. In the present work, we report, the observation of very small clusters (∼1 nm), which are in the size of interest in catalysis.

However, new electron microscopy techniques are being developed which will impact even more the study of nanoparticles.

One of them is the so-called Z-contrast which allows obtaining images of particles <1 nm (for a detailed discussion see [13]). However, this technique does not produce atomically resolved images of such small nanoparticles but allows the determination of their size and in some conditions of their geometry.

However, probably the most spectacular results will come from the use of a new generation of instruments in which the spherical aberration coefficient C_s has been corrected to an almost zero value [29]. This has already been demonstrated in practice that a sub-Angstrom resolution image of nanoparticles will become routine in the future.

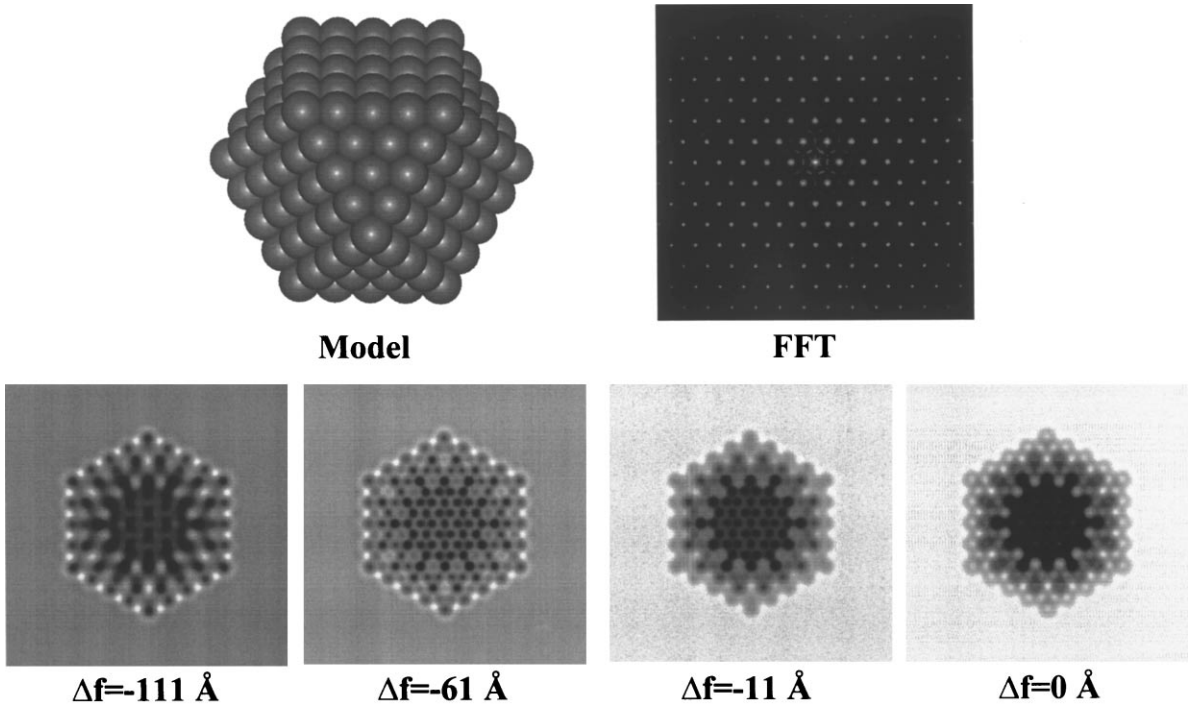

Fig. 10. Theoretical images for a cubo-octahedral particle in a zone axis ⟨1 1 1⟩ for a microscope with $C_s \sim 0$. Note that the (2 2 0) planes are clearly resolved. The corresponding defocus values are indicated in the figure.

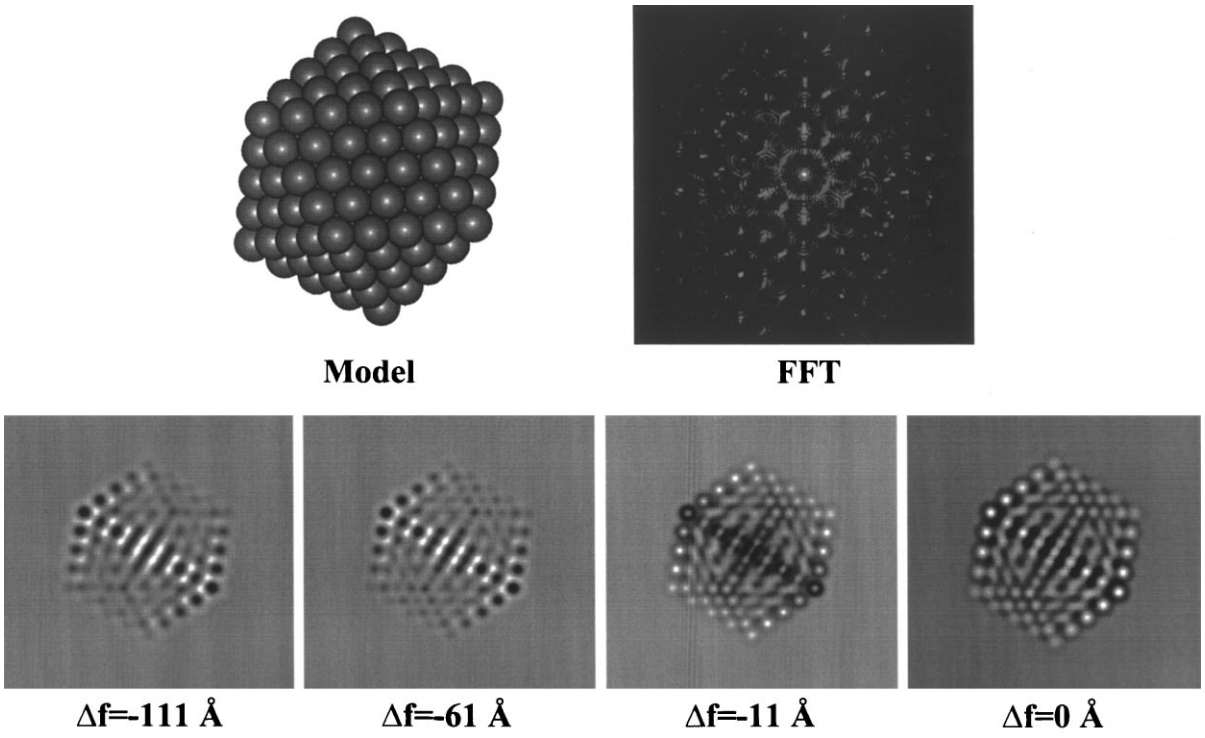

Fig. 11. Calculated images for a microscope with $C_s \sim 0$ for a particle with icosahedral shape in a two fold orientation. Note that the atoms near the edge of the particle are clearly imaged.

Many benefits are expected from those machines. First, is the ability to see (2 2 0) planes that will allow the observation of ⟨1 1 1⟩-oriented particles. This is illustrated in Fig. 10 for the case of a cubo-octahedral particle with ⟨1 1 1⟩ orientation in which the (2 2 0) planes are observed. This is a calculated image and defocus values are indicated in the figure. It should be noted that in this case the Scherzer defocus condition is meaningless and the best contrast is obtained for shorter defocus values [30].

A second example is shown in Fig. 11 for an icosahedral particle in two fold orientation it is clear that the atomic planes near the particle edge will be clearly resolved.

A final advantage will come from the fact that in all cases particles are supported on a carbon film. This produces a blurring in the high-resolution image. This effect is very difficult to avoid. However, by the use of $C_s \cong 0$ instruments that problem will be greatly reduced.

Acknowledgements

The authors are indebted to Mr. Samuel Tehuacanero and Maura Mendoza for image processing. To Mr. Luis Rendon for obtaining the high-resolution TEM images. This work was supported by CONACYT though the grant “Coloides Cuánticos y Nanopartículas”.

References

[1] R.P. Andres, S. Datta, D.B. Janes, C.P. Kubiak, R. Reifemberger, in: Han Sinsh Naiwa (Ed.), Handbook of Nanostructured Material and Nanotechnology, Vol. 4, Academic Press, New York, 2000.
[2] G.A. Somorjai, Introduction to Surface Chemistry and Catalysis, Wiley, New York, 1994.
[3] M. José-Yacamán, G. Diaz, A. Gomez, Catal. Today 23 (1995) 161.
[4] L.D. Marks, L.D. Howie, Nature 282 (1979) 196.
[5] S.J. Pennycook, D.E. Jesson, Ultramicroscopy 34 (1991) 4.

[6] J.P. Boitiaux, J. Cosyns, S. Vasudevan, Appl. Catal. 6 (1983) 41.
[7] S. Granjeaud, K. Yekache, M. Dagez, A. Humbert, C. Chapon, C.R. Henry, Microsc. Microanal. Microstru. 4 (1993) 409.
[8] H. Graoui, S. Giorgio, C.R. Henry, Surf. Sci. 417 (1998) 350.
[9] S. Giorgio, C.R. Henry, C. Chapon, C. Roucau, J. Catal. 148 (1994) 534.
[10] K. Heinemann, T. Osaka, H. Puppa, Ultramicroscopy 12 (1983) 9.
[11] J.H. Spence, Experimental High Resolution Electron Microscopy, Oxford University Press, New York, 1988.
[12] J.M. Cowley, Diffraction Physics, Elsevier, Amsterdam, 1995.
[13] Z.L. Weng, Elastic and Inelastic Scattering in Electron Diffraction and Imaging, Plenum Press, New York, 1995.
[14] M. Tomita, H. Hashimoto, T. Ikuta, H. Endoh, Y. Yokota, Ultramicroscopy 16 (1985) 9.
[15] K. Khizuka, Ultramicroscopy 5 (1980) 55.
[16] M.A. O'keefe, in: G.W. Bayley (Ed.), Proceedings of the 37th Annual Emsa Meeting, San Antonio, TX 1979, Baton Rouge, 1979, p. 556.
[17] M. Brust, M. Walker, D. Bethell, D.J. Schiffrin, R. Whyman, J. Chem. Soc., Chem. Commun. 80 (1994).
[18] H. Bönnemann, W. Brijoux, R. Brinkmann, R. Fretzen, T. Joussen, R. Köppler, B. Korall, P. Neiteler, J. Richter, J. Mol. Catal. 86 (1994) 129.
[19] L.D. Marks, Phys. Rev. Lett. 51 (1983) 1000.
[20] C.Y. Yang, M.J. Yacamán, K. Heinemann, J. Cryst. Growth 47 (1979) 283.
[21] L.D. Marks, D.J. Smith, J. Cryst. Growth 54 (1981) 425.
[22] A. Howie, L.D. Marks, Philos. Mag. 49 (1984) 95.
[23] M.J. Yacamán, J.A. Ascencio, H. Liu, J. Vac. Sci. Tech., submitted for publication.
[24] C. Cleveland, U. Landman, T.G. Schaaf, M.N. Shafigullin, P. Stephens, R.L. Whetten, Phys. Rev. Lett. 79 (1997) 1873.
[25] P. Gao, W. Kunath, H. Gleiter, K. Weiss, Scripta Met. 22 (1988) 683.
[26] I.L. Garzon, K. Michelian, M.R. Beltran, A. Posada-Amarillas, P. Ordejon, E. Artacho, D. Sanches-Portal, J.M. Soler, Phys. Rev. Lett. 81 (1998) 1600.
[27] T.P. Martin, Phys. Reports 273 (1996) 199.
[28] A. Renou, J.M. Penisson, J. Crist. Growth 78 (1986) 357.
[29] M. Haider, H. Rose, S. Uhlemann, E. Schwan, B. Tichius, K. Urban, Ultramicroscopy 75 (1998) 53.
[30] M.A. O'keefe, in: M.J. Yacamán, H. Calderon (Eds.), Proceedings of the ICEM-14 Meeting, Vol. 1, Cancún México, Institute of Physics, 1998, p. 163.